
4-1-1992

Fabry-Perot Images of NGC 1275 and Its Puzzling High-Velocity System

Adeline Caulet
NASA Goddard Space Flight Center

Bruce E. Woodgate
NASA Goddard Space Flight Center

Larry W. Brown
NASA Goddard Space Flight Center

Theodore R. Gull
NASA Goddard Space Flight Center

Paul Hintzen
NASA Goddard Space Flight Center

See next page for additional authors

Follow this and additional works at: https://scholarworks.smith.edu/ast_facpubs



Part of the [Astrophysics and Astronomy Commons](#)

Recommended Citation

Caulet, Adeline; Woodgate, Bruce E.; Brown, Larry W.; Gull, Theodore R.; Hintzen, Paul; Lowenthal, James D.; Oliverson, Ronald J.; and Ziegler, Michael M., "Fabry-Perot Images of NGC 1275 and Its Puzzling High-Velocity System" (1992). Astronomy: Faculty Publications, Smith College, Northampton, MA. https://scholarworks.smith.edu/ast_facpubs/74

This Article has been accepted for inclusion in Astronomy: Faculty Publications by an authorized administrator of Smith ScholarWorks. For more information, please contact scholarworks@smith.edu

Authors

Adeline Caulet, Bruce E. Woodgate, Larry W. Brown, Theodore R. Gull, Paul Hintzen, James D. Lowenthal, Ronald J. Oliverson, and Michael M. Ziegler

FABRY-PEROT IMAGES OF NGC 1275 AND ITS PUZZLING HIGH-VELOCITY SYSTEM

ADELINE CAULET,^{1,2,3,4} BRUCE E. WOODGATE,^{1,4} LARRY W. BROWN,^{1,4} THEODORE R. GULL,¹
 PAUL HINTZEN,^{1,5} JAMES D. LOWENTHAL,^{4,6} RONALD J. OLIVERSEN,¹ AND
 MICHAEL M. ZIEGLER^{1,4}

Received 1990 December 27; accepted 1991 October 7

ABSTRACT

We report the first images obtained with the Goddard Fabry-Perot imager, a very sensitive and tunable imaging system designed to achieve the high levels of performance required in the optical studies of faint emission-line extragalactic objects.

A velocity sequence of calibrated narrow-band CCD images (FWHM $\sim 7 \text{ \AA}$) has been obtained to cover the 3000 km s^{-1} velocity space between the redshifted $H\alpha$ emission lines of NGC 1275 (the central dominant galaxy of the Perseus Cluster), its extended associated system of low-velocity (LV) filaments and the high-velocity (HV) system of knots, projected on the same line of sight in the sky.

The lack of intermediate-velocity emission-line gas between the two systems leads to an upper limit of $1.5 \times 10^{-16} \text{ ergs cm}^{-2} \text{ s}^{-1} \text{ arcsec}^{-2}$ (3σ) on stripped ionized gas due to dynamical interaction between NGC 1275 and its high-velocity companion galaxy. It also confirms the previous reports that the level of continuum light arising from stellar or nonstellar sources must be very low in otherwise bright, strongly concentrated emission-line knots with unresolved diameters of $425 h^{-1} \text{ pc}$. The two galaxies are well separated kinematically.

We have measured the $H\alpha$ luminosities of the emission-line regions of the two systems and have derived star formation rates in order to investigate quantitatively the physical relation between the HV galaxy, NGC 1275, and the surrounding cooling flow filaments. We found that the $3'$ diameter region around NGC 1275 has a total observed $H\alpha$ luminosity of $5 \times 10^{41} h^{-2} \text{ ergs s}^{-1}$, a factor of 2.5 lower than a currently popular value (based on 1983 data). On the other hand, our measurements of central regions match other published values. Implications of this new measurement are discussed in the context of cooling flows.

Corrected for Galactic foreground absorption, the $H\alpha$ luminosity of NGC 1275 of $L_G(H\alpha) \sim 1.2 \times 10^{42} h^{-2} \text{ ergs s}^{-1}$ is comparable to those of other strong cooling flows. A normal initial mass function (IMF) for star formation in NGC 1275 is consistent with published X-ray, UV, and optical data in this paper. In particular, the revised $H\alpha$ luminosity of a strong emission-line extranuclear region can be reconciled with the limit on its continuum UV flux at 1250 \AA ; therefore, the exclusion of stars more massive than $25 M_\odot$ is no longer needed. Also, the hypothesis of a low-mass cutoff to the IMF at $2 M_\odot$, which had been introduced to reconcile the star formation rate (SFR) derived from the $H\alpha$ luminosity with the mass deposition rate of X-ray gas (\dot{M}_X), is not needed when the revised value $\text{SFR} \sim 10 h^{-2} M_\odot \text{ yr}^{-1}$ is compared with the similar value $\dot{M}_X \sim 7.5\text{--}15 h^{-2} M_\odot \text{ yr}^{-1}$ within the $30''$ radius central region.

In the HV galaxy, the $H\alpha$ luminosities of 13 regions have been measured in six narrow-band images, leading to a total observed luminosity $L(H\alpha) = 7.2 \times 10^{40} h^{-2} \text{ ergs s}^{-1}$ over a surface area of 877 arcsec^2 . The star formation rate $\text{SFR} \sim 1 h^{-2} M_\odot \text{ yr}^{-1}$ corresponds to a total stellar mass of $12 \times 10^6 h^{-2} M_\odot$ if massive stars ionize the $H\alpha$ knots. The collision of gas clouds in a heterogeneous intracluster medium with the fast-moving HV galaxy has been modeled. Following the collision, the HV interstellar medium becomes violently perturbed, with giant expanding cavities sweeping considerable masses of gas. Star formation with a $2\text{--}4 h^{-2} \%$ efficiency in the HV shocked disk supershells may occur under favorable conditions $1\text{--}8 \text{ Myr}$ after the collision event.

Subject headings: cooling flows — galaxies: individual (NGC 1275) — galaxies: interactions — galaxies: kinematics and dynamics — galaxies: Seyfert

1. INTRODUCTION

NGC 1275, the peculiar Seyfert galaxy lying near the center of the Perseus Cluster, has been the subject of numerous obser-

vational studies inspired by Minkowski's (1955, 1957) discovery of two overlapping but kinematically distinct emission-line systems ($V = 5200 \text{ km s}^{-1}$ and $V = 8200 \text{ km s}^{-1}$) near the center of the galaxy. Interest in this object was further heightened by Lynds's (1970) $H\alpha$ photograph which showed an extensive system of $H\alpha$ filaments surrounding the main body of the galaxy and lying at the redshift of the low-velocity system. Hereafter, we shall refer to NGC 1275 and gas associated with the $V = 5200 \text{ km s}^{-1}$ emission lines as the low-velocity (LV) system, and to material associated with the $V = 8200 \text{ km s}^{-1}$ complex as the high-velocity (HV) system.

Early models of NGC 1275 ascribed its peculiarities to a collision between two galaxies (Minkowski 1957) or an ex-

¹ Laboratory for Astronomy and Solar Physics, NASA/Goddard Space Flight Center, Greenbelt, MD 20771.

² NAS/NRC Research Associate; now affiliated with the Astrophysics Division, Space Science Department of European Space Agency.

³ Space Telescope European Coordinating Facility, European Southern Observatory, Karl-Schwarzschild-Strasse 2, D-8046 Garching, Germany.

⁴ Visiting Astronomers, Steward Observatory, University of Arizona, Tucson.

⁵ Department of Physics, University of Nevada, Las Vegas, NV 89154.

⁶ Steward Observatory, University of Arizona, Tucson, AZ 85721.

plosion in the galaxy's center, followed by the ejection of gaseous debris (Burbidge & Burbidge 1965; Burbidge, Smith, & Burbidge 1978). However, the subsequent detection of high-velocity H I gas seen in absorption against the NGC 1275 nucleus by De Young, Roberts, & Saslaw (1973), and extensive optical spectroscopy by Rubin et al. (1977) and by Kent & Sargent (1979), led those investigators to conclude that the HV system is a spiral galaxy falling into the center of the Perseus Cluster, with the apparent superposition of the two galaxies merely an accident of perspective. However, a plausible explanation of the phenomena in the LV system has been provided by progress in X-ray astronomy. X-ray imaging data from the *Einstein* satellite resulted in the discovery that, in some clusters of galaxies, rapid radiative energy losses from the hot, X-ray-emitting gas, 10^7 – 10^8 K, would result in a flow of cooling gas toward the cluster center (see review by Sarazin 1988). The X-ray data strongly indicate the presence of such a cooling flow around NGC 1275. The resulting coalescence of cool 10^4 K gas could explain the LV H α filaments observed by Lynds, the extended LV H α emission near the center of NGC 1275, and the presence of a young stellar component in this elliptical galaxy (Fabian & Nulsen 1977; Romanishin 1987; Shields & Filippenko 1990).

Because the interstellar medium (ISM) of a spiral galaxy would not be expected to survive an encounter with the dense intracluster material near the center of the Perseus Cluster, it was generally assumed that the LV and the HV systems were not physically interacting (Rubin et al. 1977). However, Hu et al. (1983) disagree, suggesting that a collision between the HV foreground galaxy and the LV gas associated with NGC 1275 is needed to explain the unusually high H α luminosity of the LV system, which was at least 4 times that of other cooling flow systems known at that time. Though they also note problems with the interaction model, Hu et al. cite as support "a striking [spatial] correspondence between the brighter regions of the low velocity emission and the high velocity filament." Unger et al. (1990), who published Fabry-Perot imaging data of the HV system, note that most of the HV emission is in two distinct regions, neither of which overlaps the NGC 1275 nucleus, but they conclude that this anticorrelation between HV and LV emission also supports the interaction model. Hu et al. postulate a high-temperature shock in order to explain the apparent lack of intermediate velocity optical emission lines, in the range 5200–8200 km s $^{-1}$, from slipstream material entrained by the HV galaxy as a result of the postulated collision. Nevertheless, they conclude that the lack of such emission is puzzling.

In this paper we present Fabry-Perot H α images of the HV and LV systems. Our measurement of the total H α luminosity of NGC 1275 is a factor of ~ 2.5 lower than the value derived by Cowie et al. (1983). On the other hand, our emission-line fluxes agree well with other previous measurements, spectroscopic and imaging (Kent & Sargent 1979; Heckman 1981), when comparing the same surface areas. In addition, the LV H α flux is no longer discordant with other known luminous cooling flow objects. The H α luminosities we derive for the individual HV clouds (knots) are similar to those observed in nearby spiral galaxies (Kennicutt 1983; Kennicutt & Kent 1983), strengthening the argument that the HV system contains giant H II regions like those in a normal Sc or Scd spiral galaxy (Rubin et al. 1977) or in the Large Magellanic Cloud (LMC) (Meaburn et al. 1989). Our measurements on H α emission at velocities between the HV and LV systems yield an upper limit

on emission from slipstream gas which implies that the orbit of the HV system has not gone through the central core of the cluster or that the HV galaxy is not interacting with the cooling flow anywhere near NGC 1275. The observed H α luminosities in the HV knots indicate the presence of thousands of young ionizing stars that were possibly formed a few Myr after the collision of the HV galaxy with intracluster medium (ICM) clumps comoving in the cluster cooling flow.

2. THE INSTRUMENT AND OBSERVATIONS

The observations, made on 1988 November 22 and 23 at the Steward Observatory 2.3 m telescope, yield the first results obtained with the Goddard Fabry-Perot imager (GFPI). The system consists of a piezoelectric gap scanning etalon and a servocontroller, both made by Queensgate Instruments, Ltd., of blocking filters and a Tektronix CCD detector. The GFPI configuration used for these observations is found in Table 1. The resolution chosen for these observations corresponds to ~ 330 km s $^{-1}$ at H α in the rest frame of the objects. The etalon was scanned over the wide velocity range of 3000 km s $^{-1}$ that separates the two velocity systems along the line of sight of NGC 1275.

Figure 1 shows the instrument layout. The three-period blocking filter is placed in the collimated beam and eliminates all but one interference order. Internal reflections occur between the leading surface of the interference filter and the back side of the etalon and give rise to a series of multiple images next to the primary image. Each filter with multilayered, not antireflective coatings creates its own ghost pattern which can be easily recognized in the standard or focus star fields taken through the same filter. These reflections appear always at the same separation and orientation with respect to the source, often in blank sky regions on our CCD frames, and could be easily distinguished from real objects.

TABLE 1
GFPI CONFIGURATION IN THIS PAPER

Parameter	Value
Instrument	
Telescope aperture (m)	2.29
Cassegrain ratio	f/9
Focal lengths:	
Collimator, f_{coll} (mm)	300
Camera, f_{cam} (mm)	200
Output beam	f/6
Detector	
CCD Tek, thinned format (pixels)	512 \times 512
Pixel size, p_{μ}	27 $\mu\text{m} = 0''.406$
Field size	208" \times 208"
Binning factor	1
Peak Q.E.	50% at H α
Readout noise	10e $^{-}$ rms
Gain	3.8e $^{-}$ /DN
Etalon	
QI serial	ET 50-835
λ (Å)	5550–7050
FSR (Å)	166.4 at 6456 Å
Finesse, N_e	22.4
Order	38
Etalon gap	12.7 μm at 6615 Å
Resolution	7.4 Å at 6456 Å = 344 km s $^{-1}$
Resolucance, R_{λ}	872

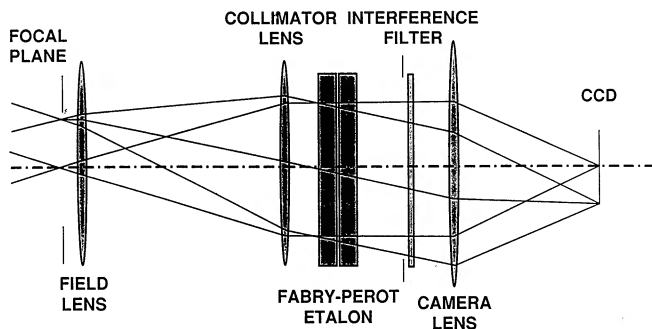


FIG. 1.—Optical layout for the Goddard Fabry-Perot imager. The on-axis and extreme rays are drawn passing through the field and collimator lenses, the Fabry-Perot etalon, the interference blocking filter, and the camera lens. They form an image at the focal plane on the CCD detector.

The wavelength calibration is obtained by scanning the emission lines from spectral lamps. The etalon and filters are thermally controlled to within 0.5°C to minimize wavelength drift; small drifts, if they occur, are corrected in the calibration relation, by measuring the drift offset of a standard emission line. This check was done twice each night; no appreciable drift in the optical gap occurred throughout the nights. In its present configuration, the GFPI produces nearly monochromatic images. We have measured a wavelength shift of less than 1 \AA at $r \sim 128$ CCD pixels, where r is the radial distance from the optical axis. At the CCD edges, the shift is 3.8 \AA (0.5 FWHM). The objects studied in this paper are imaged on the “monochromatic” area of the CCD frames.

The observations are summarized in Table 2. The GFPI was tuned at wavelengths λ_c corresponding to the object redshifted emission lines. The CCD frames were bias-subtracted and flat-fielded as usual, with standard IRAF routines. For all frames, the sky illumination was mapped by masking the extended objects and fitting a low-order cubic spline to the sky background. Each background map was subtracted from the corresponding frame. The cosmic-ray hits were removed from each image. The flux calibration was derived from CCD exposures of the photometric standard stars, Hiltner 600 and Feige 110, with the GFPI tuned at or near the observed wavelengths λ_c of the object frames (Massey et al. 1988). After correction of the data for air mass using the mean standard KPNO extinction curve, the photometric calibration was done with an error less than 10% in magnitude. The overall throughput quantum efficiency (Q.E.) (telescope, instrument, and CCD) is very good, $\sim 16\%$ at 6600 \AA (Table 2). All images were registered to a common spatial position and scaled to absolute fluxes. Images taken in the same bandpass were combined. Two continuum frames at $\lambda_c = 6720$ and 6728 \AA were co-added, then scaled to each object frame and subtracted from it. The scaling factors were derived from the average amplitude of the point-spread functions (PSFs) of five field stars. The PSFs, which were constructed from two-dimensional elliptical Gaussian fits to the stars, indicate that the seeing was $1''.7$ – $1''.8$. The seeing differences between frames could not be easily corrected and produced residual stellar images in the continuum-subtracted images.

3. OBSERVATIONAL RESULTS

3.1. Images and Morphology of the Two Systems

The continuum and emission-line fluxed images are presented in Figures 2a–2p (Plates 1–4) showing the central $1/8$

$\times 1/7$ area of the CCD frames. Starting with the LV system in $\text{H}\alpha$, then in $[\text{N II}] \lambda 6584$, the sequence covers 3550 km s^{-1} between the two velocity systems in coarse steps of $\sim 330 \text{ km s}^{-1}$, and ends with the LV system in $[\text{S II}] \lambda \lambda 6716, 6731$. The images in Figures 2i–2n were taken every $\sim 165 \text{ km s}^{-1}$ and give more detail on the HV system $\text{H}\alpha$ gas kinematics.

The full-size CCD images encompass a $\sim 3' \times 3'$ field [$1' = 15 h^{-1} \text{ kpc}$, $h = H_0 (100 \text{ km s}^{-1} \text{ Mpc}^{-1})^{-1}$]. The long $\text{H}\alpha$ filaments observed by Lynds (1970) are seen; on our images, the filaments appear clumpy. The NGC 1275 filamentary system extends up to 4 arcmin (Lynds 1970). The brighter regions are detected in all lines ($\text{H}\alpha$, $[\text{N II}]$, $[\text{S II}]$), including the emission-line filament studied by Shields & Filippenko (1990) and the jetlike structure pointing westward from the nucleus, visible on the color $\text{H}\alpha$ plate of Cowie et al. (1983). We see a round knot along this jetlike structure at $\sim 6''$ northwest from the nucleus and a position angle (P.A.) $\sim 284^\circ$. The extended region of $\sim 8''$ radius around the nucleus emits a substantial amount of line flux and has a complex morphology: besides the jetlike structure, bright wisps emerge from the elongated main body, some going in the direction of the outer filaments. The nuclear features change aspect from one velocity frame to another (see Figs. 2c–2f).

The images in Figures 2i–2n show new details on the HV

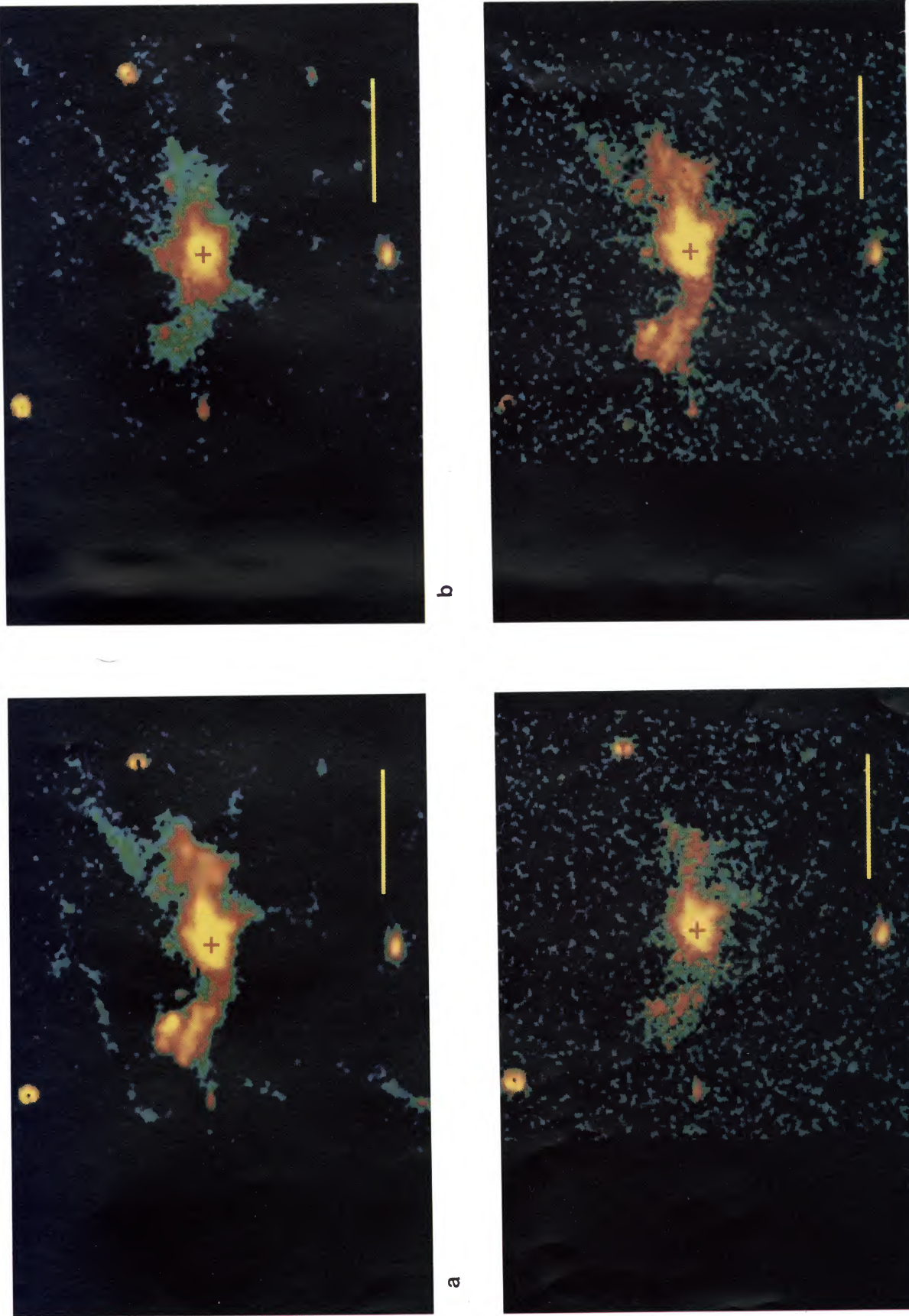
TABLE 2
SUMMARY OF OBSERVATIONS
A. NGC 1275

Fig. 2 Index	Combined Exposure (s)	λ_c (\AA)	V (km s^{-1})	Description
a	4800	6676.2	5184	$\text{H}\alpha$ LV on line
b	2400	6683.6	5522	$\text{H}\alpha$ LV red wing
c	600	6690.6	4876	$[\text{N II}] \lambda 6584$ LV blue wing
d	600	6698.1	5218	$[\text{N II}] \lambda 6584$ LV on line
e	600	6705.5	5555	$[\text{N II}] \lambda 6584$ LV red wing
f	600	6712.9	5892	$[\text{N II}] \lambda 6584$ LV red wing
g	600	6720.4	...	Continuum
h	600	6727.8	...	Continuum
i	2400	6734.5	7849	$\text{H}\alpha$ HV blue wing
j	600	6739.0	8054	$\text{H}\alpha$ HV blue wing
k	2400	6741.9	8187	$\text{H}\alpha$ HV on line
l	600	6746.4	8393	$\text{H}\alpha$ HV on line
m	600	6750.1	8562	$\text{H}\alpha$ HV red wing
n	600	6753.9	8736	$\text{H}\alpha$ HV red wing
o	600	6832.2	5172	$[\text{S II}] \lambda 6716$ LV on line
p	600	6846.3	5149	$[\text{S II}] \lambda 6731$ LV on line

B. CALIBRATION STARS^a

Star	λ_c (\AA)	Air Mass	Q.E. (%)
Feige 110	6583.0	1.40	15.3
	6599.9	1.43	18.5
G191B2B	6675.7	1.43	15.4
	6698.1	1.46	16.5
	6742.7	1.48	15.0
	6832.2	1.51	17.8
Hiltner 600	6599.6	1.28	17.4
	6676.2	1.19	16.0
	6683.6	1.20	16.3
	6699.5	1.31	17.2
	6734.5	1.23	17.6
	6741.9	1.22	16.0
	6799.4	1.34	20.0

^a Exposure 60 s.

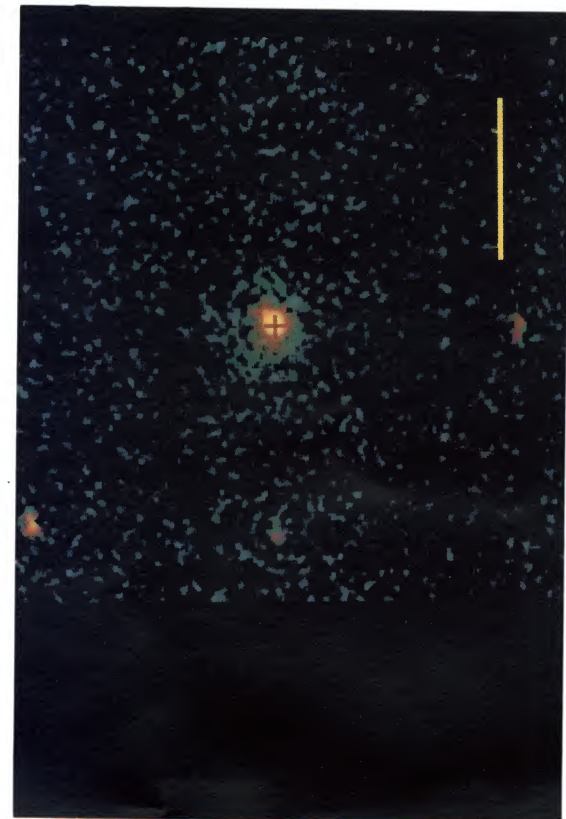


FIGS. 2*a-d*

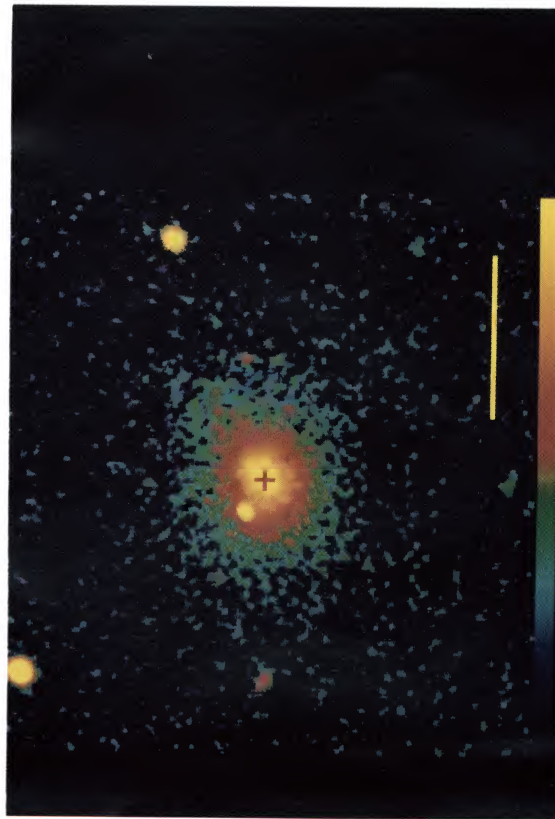
FIG. 2.—(*a-p*) Intensity color-coded images of the 5200 km s^{-1} (LV) and 8200 km s^{-1} (HV) systems around NGC 1275 in the Perseus Cluster. A 3×3 boxcar mean smoothing and a color-coded logarithmic display are used to enhance the contrast. The surface brightness-colorrelation is represented by the color bar at the bottom of (*b*), from a lower limit of -16.5 (blue) to an upper limit of -15 (yellow), in log units of $\text{ergs cm}^{-2} \text{ s}^{-1} \text{ arcsec}^{-2}$. The plate scale is indicated by the $30''$ length yellow bar (horizontal axis). The north and east directions are $\sim 2^\circ$ counterclockwise from the vertical (*top*) and horizontal (*left*) axis respectively. A plus sign (+) indicates the position of the Seyfert nucleus. Note a few residual stars and Fabry-Perot reflections which occur for bright sources. A ghost, $\sim 1.5''$ southwest from the Seyfert nucleus, lies upon [S II] emission. A continuum frame, combining images *g* and *h*, has been subtracted from images *a-f* and *i-p* (see Table 2 for description).

CAULET et al. (see 388, 303)

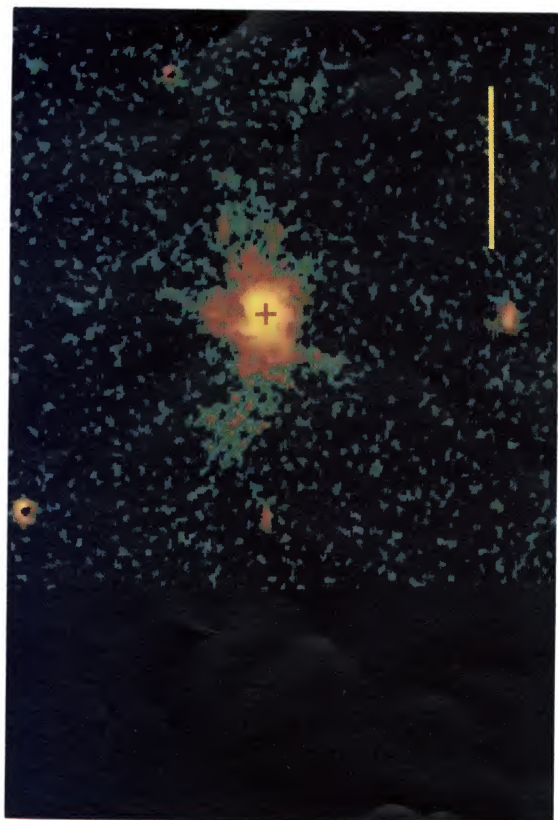
PLATE 2



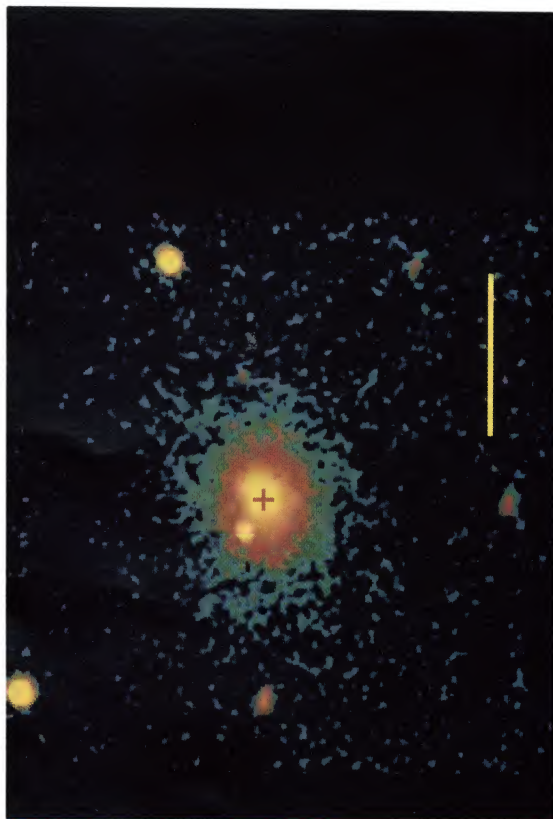
f



h



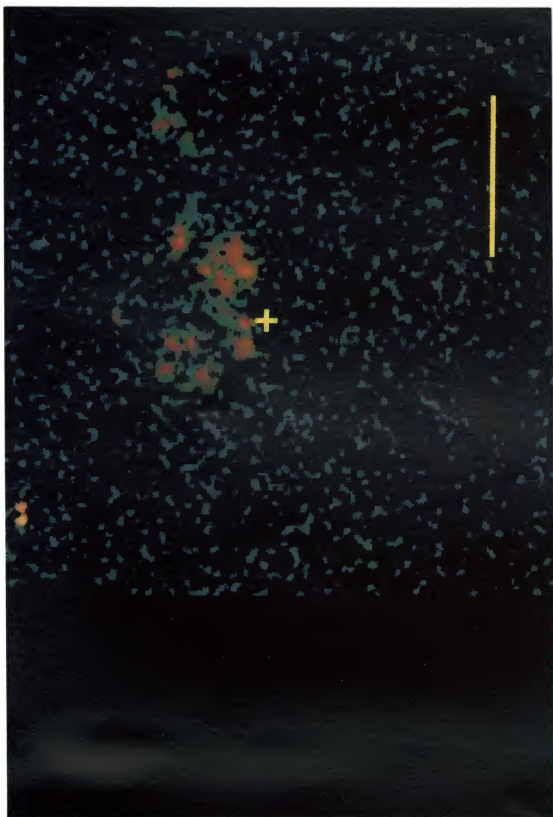
e



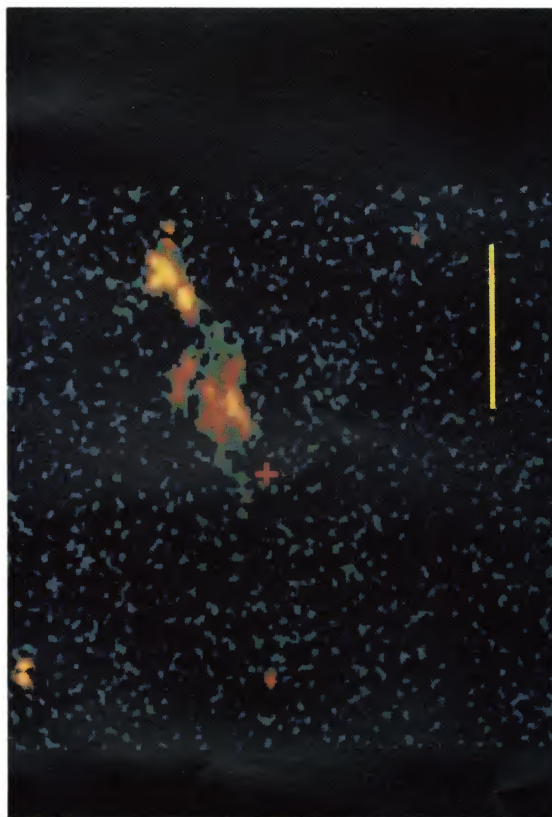
g

FIG. 2e-2h

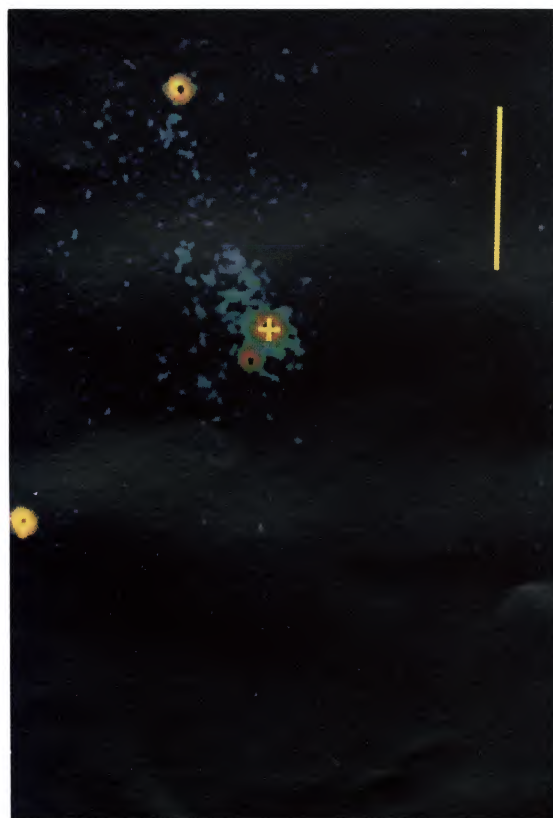
CAULET et al. (see 388, 303)



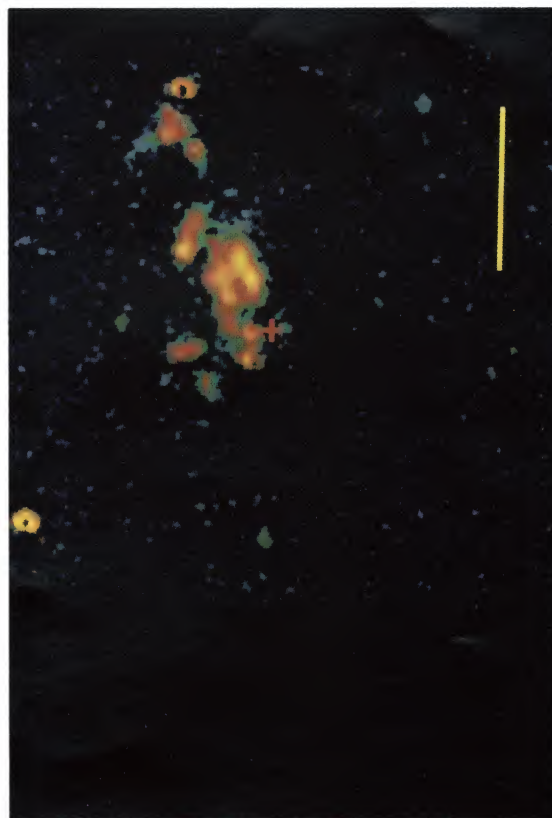
j



i



k



l

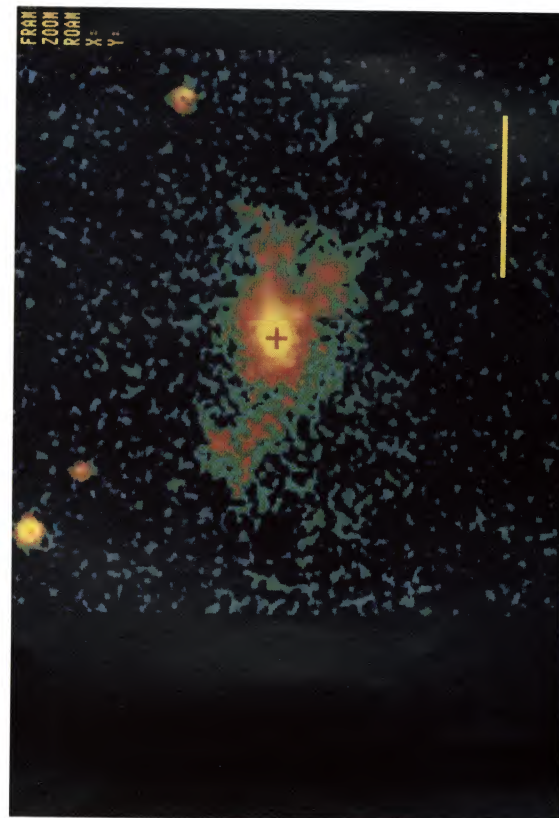
Figs. 2i-2l

CAULET et al. (see 388, 303)

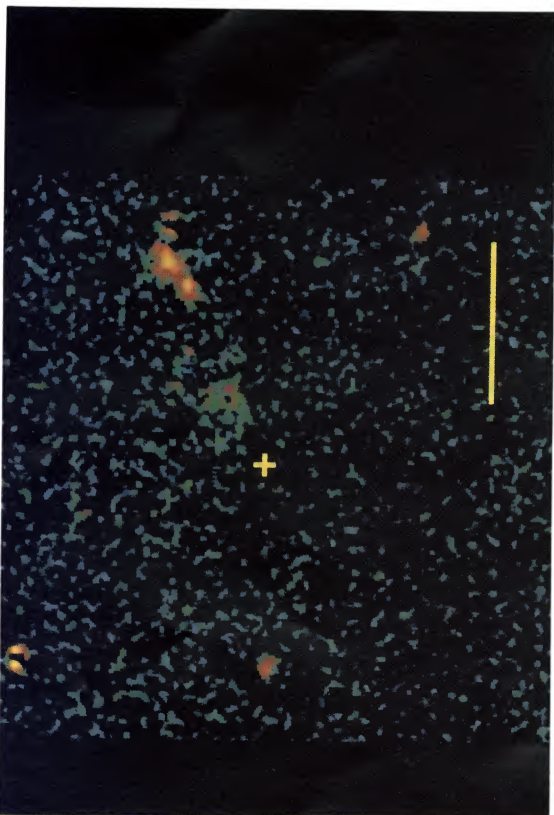
PLATE 4



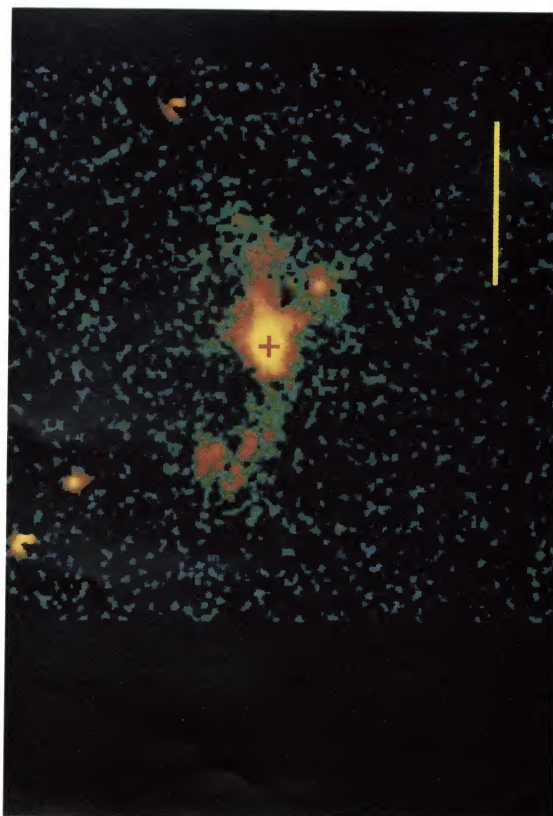
n



p



m



o

Figs. 2*m*-2*p*

CAULET et al. (see 388, 303)

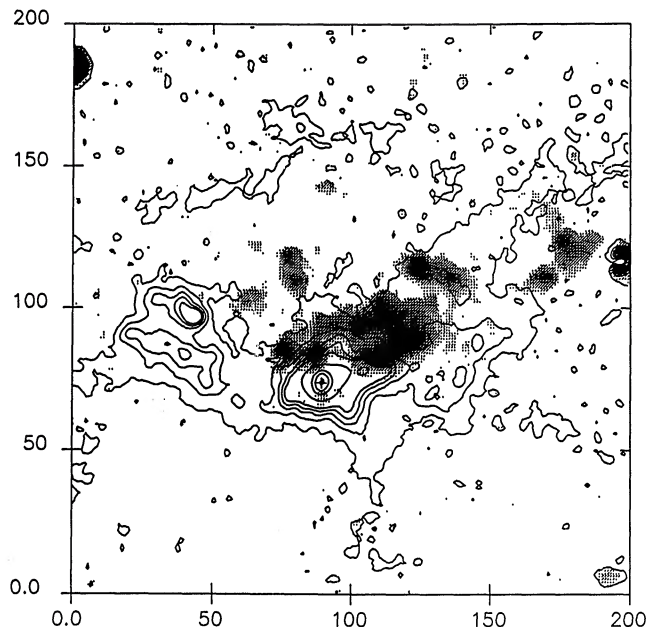


FIG. 3.— $H\alpha$ surface brightness contours of the LV system (Fig. 2a) superposed on the $H\alpha$ image of the HV system (Fig. 2k). The contour levels are 5 (1σ), 25, 45, 65, 85, 200, 700, 1200, 1700, in units of 10^{-17} ergs cm^{-2} s^{-1} arcsec^{-2} . Axis (in pixels, $0''.406$ pixel $^{-1}$), orientation, and position of the nucleus *plus sign* as in Fig. 2.

system. Bright $H\alpha$ knots, unresolved at $\sim 1''.8$ seeing, are well defined and surrounded by extended fainter emission. The knots tend to form pairs or chains along the overall east–west direction of NGC 1275 and of the Perseus Cluster. Figure 3 shows $H\alpha$ surface brightness contours of the LV system superposed on the $H\alpha$ image of the HV system. The latter is located on the north side of the main body of NGC 1275, mostly to the west. A few HV knots are not projected upon any extended emission from the LV system (knots 1, 2, 10, and 11 identified in Fig. 4).

3.2. Fluxes

In this paper, we are using a distance of $55 h^{-1}$ Mpc for both systems (Cowie et al. 1983). The $H\alpha$ and $[\text{N II}]$ images of the LV system taken at the same velocities show similar structures. Examination of Figures 2g and 2h, which would correspond to $H\alpha$ between the LV and HV systems, reveals no extended emission. Thus, there is no evidence for any $H\alpha$ emission-line gas at any intermediate velocity between the LV and HV systems, which could have been attributed to $H\alpha$ emission from slip-stream ionized gas due to an interaction between the two systems. The continuum image (Figs. 2g and 2h combined) yields an upper limit of 1.5×10^{-16} ergs cm^{-2} s^{-1} arcsec^{-2} (3σ) on the $H\alpha$ surface brightness emission from the putative intermediate-velocity gas. Neither Rubin et al. (1977) nor Kent & Sargent (1979) had detected gas spectroscopically at intermediate velocities. Recently, Meaburn et al. (1989) reported the detection of continuum light at 5200 \AA from a $20''$ long faint filament going through the HV knots 10 and 11. We estimate a $\sim 2''$ width for the filament; then the intensity quoted by the authors corresponds to a surface brightness of 8.4×10^{-17} ergs cm^{-2} s^{-1} arcsec^{-2} , which is slightly below our detection limit. Emission-line-free exposures of better sensitivity would be of great interest to confirm Meaburn et al.'s observations,

and to search for other continuum regions associated with the gaseous emission knots.

Our $H\alpha$ flux measurements for the two systems are presented in Tables 3 and 4. For the LV system, fluxes were measured in each 25×25 pixel square of a grid centered on the nucleus. The luminosity limit for reporting detections above 3σ in each grid element is $0.225 \times 10^{39} h^{-2}$ ergs s^{-1} . Residual stars or instrumental ghosts were not included. With an image every FWHM, the line fluxes are obtained by adding the fluxes from all images that cover the line (Figs. 2a and 2b for $H\alpha$, Figs. 2c–2f for $[\text{N II}]$). We have to correct empirically our values of the $H\alpha$ flux, because we do not have an observation of the LV $H\alpha$ blue wing: we have assumed for the $H\alpha$ blue wing the same contribution as the $H\alpha$ red wing. Table 3 shows a good agreement, within the $\sim 10\%$ errors, between our line measurements and all published fluxes inside a $35''$ radius around the NGC 1275 nucleus. However, Cowie et al. (1983) derived an $H\alpha$ line flux for their whole $4.5'$ field, a factor ~ 2.9 greater than our flux measurement in the main region. The flux emitted by all filaments outside the main region which contains the luminous galactic body cannot possibly exceed the flux from the main region; we estimate its $H\alpha$ contribution above 3σ to be only 14% of that region. In Table 3 the line luminosities of our whole field (total region) include those of the main region and all filaments outside the main region detection in the CCD $H\alpha$ frames. For comparison with the $H\alpha$ fluxes, we did not include additional emission in the $[\text{N II}]$ or $[\text{S II}]$ images from objects which were not detected in the $H\alpha$ images. We have also examined the color-coded surface brightness levels of the $H\alpha$ image of Cowie et al. (their Fig. 3a; 20 \AA bandwidth) and the composite $H\alpha$ image of Hu et al. (1983; their Fig. 2c) formed by adding together their continuum-subtracted narrow-band frames for comparison with the Cowie et al. broader frame. The results of Hu et al. are in better agreement with ours. Outside the main

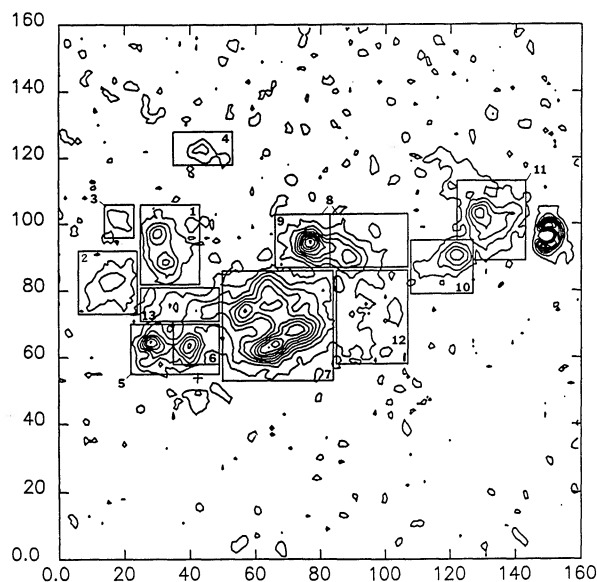


FIG. 4.— $H\alpha$ surface brightness contours of the HV system (Fig. 2k). Spacing between the nine plotted contours is 10^{-16} , with the lowest contour plotted at the 1σ level, i.e., 5×10^{-17} (in units of ergs cm^{-2} s^{-1} arcsec^{-2}). Thirteen emission-line regions with fluxes in Table 4 are located on the contour plot. Axis (in pixels), orientation, and position of the nucleus (*plus sign*) as in Fig. 2.

TABLE 3
LV SYSTEM EMISSION-LINE LUMINOSITIES
($10^{39} h^{-2} \text{ ergs s}^{-1}$; not dereddened)

Region ^a	H α		H α	[N II] λ 6584	[S II] λ 6716	[S II] λ 6731	Reference
	Partial ^b				Partial ^c	Partial ^c	
Central	219 (± 15)	314 ^d (± 21)	316 (± 21)	51 (± 3)	65 (± 3)	1	
Main	300 (± 19)	417 ^d (± 27)	424 (± 30)	76 (± 5)	103 (± 6)		
Total	340 (± 24)	475 (± 33)	460 (± 36)	81 (± 6)	111 (± 7)		
Cluster	4.7 (± 0.6)	5.6 (± 0.7)	4.1 (± 0.5)	1.0 (± 0.1)	1.0 (± 0.1)		
R163	16.9 (± 0.9)	20.6 ^d (± 1.0)	18.1 (± 1.0)	4.7 (± 0.2)	4.4 (± 0.2)		
Central	...	208.8 ^e	2	
Main	...	450.0 ^f	3	
Total	...	1200.0	4	
Cluster	...	6.6 ^g	5	

^a *Central*: from a region of size $30''.5 \times 30''.5$ centered on the nucleus. *Main*: from a region of size $71'' \times 71''$ centered on the nucleus; Heckman considers nearly the same region of $30''$ radius. *Total*: (this paper) from a region of size $172''.6 \times 172''.6$ centered on the nucleus, including the main region and those filaments beyond, which are detected in H α (Figs. 2a and 2b). Cowie et al. 1983 considers the same region, but with a 4.5 diameter. *Cluster*: bright knot of size $3''.7 \times 3''.7$ located $21''$ from the nucleus at P.A. = $61^\circ 4'$, to compare with Shields & Filippenko's cluster region (seen on their Fig. 1b). *R163*: extended region around the cluster, of size $10''.2 \times 10''.2$ centered at $22''.9$ from the nucleus at P.A. = $61^\circ 4'$.

^b Obtained by adding values from H α images (Figs. 2a and 2b).

^c Partial line luminosity (Figs. 2o and 2p). In addition, [S II] λ 6716 emission from the red-line wing seems to contribute some flux in the [S II] λ 6731 line (Fig. 2p). The flux from a 25×25 pixel region around a ghost located $\sim 15''$ southwest from the Seyfert nucleus was excluded from these measurements.

^d Assuming that the contributions from the H α blue wing (no observation), and H α red wing (Fig. 2b) are equal (see text).

^e Derived from Kent & Sargent's mean H β flux of $1.3 \times 10^{-16} \text{ ergs cm}^{-2} \text{ s}^{-1} \text{ arcsec}^{-2}$ and a ratio H α /H β = 4.77 (not dereddened). This is comparable to our own mean estimate of 1.96×10^{-16} . We have assumed that the listed $I(\text{H}\beta)$ value of Kent & Sargent's Table 3 was in fact the $F(\text{H}\beta)$ value not corrected for reddening, since otherwise the inferred central H α luminosity would be ~ 6.7 times lower than our value.

^f From Heckman's 1981 H α + [N II] λ 6584 measurement, and $L(\text{H}\alpha) = L([\text{N II}])$.

^g Obtained from Shields & Filippenko's extinction-corrected flux of $5 \times 10^{-14} \text{ ergs cm}^{-2} \text{ s}^{-1}$, a total extinction $A_V = 1.34$ mag, and mean extinction curve of Cardelli, Clayton, & Mathis 1989.

REFERENCES.—(1) This paper; (2) Kent & Sargent 1979; (3) Heckman 1981; (4) Cowie et al. 1983; (5) Shields & Filippenko 1990.

region, 60 grid elements, out of a total of 223, have fluxes larger than 3σ . Therefore, it seems reasonable to consider a value of $550 \times 10^{39} h^{-2} \text{ ergs s}^{-1}$ as an upper limit for the total H α flux. Thereafter, we will adopt our own value, $L(\text{H}\alpha) \sim 5 \times 10^{41} h^{-2} \text{ ergs s}^{-1}$. New narrow-band observations covering the blue wing of the H α line are needed to improve the accuracy of

this result. The astrophysical implications of this new measurement are discussed in the next section.

Fluxes for each HV narrow-band image are given in Table 4. Measurements were done as those for the LV images; 13 individual emission-line regions were defined to cover all bright knots and extended nebosity. Their locations are represented

TABLE 4
HV SYSTEM H α LUMINOSITIES
($10^{39} h^{-2} \text{ ergs s}^{-1}$; not dereddened)

REGION ^a	SIZE (arcsec ²)	NARROW-BAND λ_c (Å)						TOTAL H α ^b
		6734.5	6739.0	6741.9	6746.4	6750.1	6753.9	
1.....	7.7 \times 10.2	0.73	2.00	2.37	...	0.77	...	3.9 \pm 0.3
2.....	7.7 \times 8.1	0.74	1.80	1.19	...	0.30	...	2.2 \pm 0.2
3.....	4.1 \times 4.5	0.20	0.78	0.23	...	0.22	...	0.64 \pm 0.09
4.....	7.7 \times 4.5	0.21	0.47	0.41	...	0.18	...	0.47 \pm 0.06
5.....	11.4 \times 6.5	...	2.59 ^c	4.26 ^c	1.03	0.52	...	4.8 \pm 0.4
6.....	6.1 \times 5.3	...	1.14	2.17	0.43	0.29	...	2.5 \pm 0.2
7.....	14.2 \times 13.8	3.49	7.52	18.07	11.58	3.65	1.90	25.2 \pm 1.0
8.....	17.1 \times 6.9	1.26	2.43	5.05	3.09	1.60	...	7.9 \pm 0.5
9.....	7.3 \times 6.9	0.71	1.61	3.16	1.36	0.78	...	4.6 \pm 0.4
10.....	8.1 \times 6.9	0.58	0.83	1.47	5.43	2.26	0.67	6.9 \pm 0.7
11.....	83.7	1.07	1.58	3.97	9.51	4.90	1.26	12.3 \pm 1.4
12.....	9.3 \times 11.8	0.92	1.02	1.97	3.52	1.05	0.39	4.9 \pm 0.4
13.....	10.2 \times 4.5	0.56	1.10	1.70	0.26	0.21	...	2.5 \pm 0.2

NOTE.—No value (...) reported when below the 3σ detection limit, which corresponds to $1.5 \times 10^{-16} \text{ ergs cm}^{-2} \text{ s}^{-1} \text{ arcsec}^{-2}$ (i.e., $9 \times 10^{36} \text{ ergs s}^{-1} \text{ pixel}^{-1}$).

^a Location of regions on Fig. 4.

^b See text for adding individual narrow-band fluxes.

^c Contamination by a foreground star?

on the HV contour plot (Fig. 4). The plate sequence was done every 0.5 FWHM; the $H\alpha$ line fluxes are obtained by adding flux values every FWHM, including each region peak flux. There are few published measurements on the HV system to compare with ours. From their mean $H\alpha$ spectroscopic value, Kent & Sargent (1979) derived $3 \times 10^{40} h^{-2} \text{ ergs s}^{-1}$ for 375 arcsec² which is in agreement with our observed $H\alpha$ luminosity of $7.2(\pm 0.5) \times 10^{40} h^{-2} \text{ ergs s}^{-1}$ over a total surface area of 877 arcsec² including all distinct regions listed in Table 4 (regions 1–5, 7, 8, 10–13). Meaburn et al. (1989) observed [O III] $\lambda 5007$ luminosities of 2.7 and $5.8 \times 10^{39} h^{-2} \text{ ergs s}^{-1}$ in two regions of 12 and 45 arcsec² centered on knots 10 and 11, respectively. For the same size regions, we obtain $H\alpha$ luminosities of $5.2(\pm 0.6)$ and $11.0(\pm 0.8) \times 10^{39} h^{-2} \text{ ergs s}^{-1}$; thus, the observed [O III] $\lambda 5007/H\alpha$ ratio is ~ 0.5 in these regions, in fair agreement with Kent & Sargent's mean spectroscopic line ratio of 0.8 across the HV system (from their Table 2). The HV system has little intrinsic reddening (Kent & Sargent 1979). In this paper, we use the mean extinction relations derived by Cardelli, Clayton, & Mathis (1989) to correct fluxes for reddening. After correction for Galactic foreground extinction only ($A_V = 0.54$ mag; Burstein & Heiles 1984), and using the radiative recombination value $H\alpha/H\beta$ of 2.85, the line ratio [O III] $\lambda 5007/H\beta$ would be 1.7 in these regions. This is compatible with values of this ratio being less than 3 in most starburst and H II region galaxies (Osterbrock 1989).

Unger et al. (1990) observed the HV system in the [O III] emission line at $\sim 60 \text{ km s}^{-1}$ resolution; they found evidence for peculiar velocity structure in the HV system, and suggested that this galaxy has been perturbed. Our observations show a smooth change in velocity from east to west (Figs. 2i–2n). The $H\alpha$ emission in the HV system peaks over a velocity range of $\sim 340 \text{ km s}^{-1}$ (Table 4), in agreement with Rubin et al.'s (1977) observations. The observed FWHM $\sim 10.6 \text{ \AA}$ of the $H\alpha$ emission line of the whole HV system was obtained by fitting a Gaussian, centered at 6743.7 \AA , through the six narrow-band total fluxes (from Table 4). After correction for the instrumental width of 7.4 \AA , this corresponds to an intrinsic FWHM $\sim 338 \text{ km s}^{-1}$ in the HV rest frame, typical of a rotating galaxy, in agreement with Rubin et al.'s conclusions.

4. NGC 1275 REVISED $H\alpha$ LUMINOSITY AND IMPLICATIONS FOR COOLING FLOWS

We found that the observed total $H\alpha$ luminosity of the filaments around NGC 1275 is $L(H\alpha) \sim 5 \times 10^{41} h^{-2} \text{ ergs s}^{-1}$, reducing Cowie et al.'s (1983) previous estimate by a substantial factor of ~ 2.5 . NGC 1274 was viewed as an exceptionally luminous emission-line system among other rich, X-ray luminous clusters. Correcting our value of $L(H\alpha)$ for Galactic foreground extinction ($A_V = 0.54$ mag; Burstein & Heiles 1984), the total revised $H\alpha$ luminosity for NGC 1275 becomes $L_G(H\alpha) = 7.5 \times 10^{41} h^{-2} \text{ ergs s}^{-1}$. This is comparable to the extinction-corrected $H\alpha$ luminosities of other strong cooling flows, such as PKS 0745–191 [$L_G(H\alpha) \sim 1.2 \times 10^{42} h^{-2} \text{ ergs s}^{-1}$; Romanishin 1987], A2597 and A1795 (~ 7.6 and $2.3 \times 10^{41} h^{-2} \text{ ergs s}^{-1}$; Heckman et al. 1989), 2A 0335+096 ($\sim 2.8 \times 10^{41} h^{-2} \text{ ergs s}^{-1}$; Romanishin & Hintzen 1988). These are characterized by a high mass accretion rate \dot{M}_X of hot intracluster gas onto large emission-line nebulae, with an overall low ionization state of the filaments. Additional correction for intrinsic reddening ($A_V = 0.80$ mag; Shields & Filippenko 1990) leads to $L_0(H\alpha) = 1.4 \times 10^{42} h^{-2} \text{ ergs s}^{-1}$ for NGC 1275. To establish better correlations between the

optical nebulae and the X-ray cooling gas, it would be helpful to determine the intrinsic extinction for a large sample of cooling flows (e.g., Heckman et al.'s 1989 sample).

For NGC 1275, the revised $L(H\alpha)$ value helps us resolve several issues discussed recently by Johnstone & Fabian (1988). One central problem concerns the excitation and heating sources of the emission-line clouds. A wide variety of possibilities have been considered, "without finding a clear winner" (Heckman et al. 1989); this is not surprising in view of the large scatter between $L_G(H\alpha)$ and \dot{M}_X among cooling flows. In NGC 1275, Johnstone & Fabian's model of photoionization by the active nucleus can now account for the extinction-correction revised luminosity $L_0(H\alpha)$; the line emission is concentrated in the central 10" diameter region, where the nucleus is likely to be the dominant ionization source. But there is also evidence for distributed sources of ionization, such as the young star-forming region found by Shields & Filippenko (1990; noted cluster in our Table 4), where the line emission is characteristic of H II regions and has a higher ionization state than in the surrounding filaments; in the cluster region, these authors note that there is a blue continuum source, and star formation seems to occur according to a normal initial mass function (IMF) appropriate to disk galaxies. Another strong emission-line, extranuclear region puzzled Johnstone & Fabian, who hypothesized an IMF truncated at a low upper mass cutoff to reconcile the $H\alpha$ luminosity in this region, which they estimated from the plates of Cowie et al. (1983), with the limit on the continuum ultraviolet flux at 1250 \AA . In this 10" \times 10" region, located 10" southeast from the nucleus at P.A. 103 $^\circ$ 8, we find $L_0(H\alpha) = 7 \times 10^{40} h^{-2} \text{ ergs s}^{-1}$, which is at least a factor of 3 lower than Cowie et al.'s corresponding value (using Galactic + internal $A_V = 1.34$ mag; Kent & Sargent 1979; Shields & Filippenko 1990). This leads to a total star formation rate (SFR) = $0.6 h^{-2} M_\odot \text{ yr}^{-1}$ in this region, assuming photoionization by a stellar population with a standard IMF (Kennicutt 1983). We predict a continuum flux, reddened, of $\sim 2 \times 10^{-16} h^{-2} \text{ ergs cm}^{-2} \text{ s}^{-1} \text{ \AA}^{-1}$ at 1250 \AA , which is below the IUE 2 σ detection limit ($\sim 2.5 \times 10^{-16}$). Therefore, no upper mass cutoff is required, unless the reddening in this region is much less than our adopted value.

Similarly, using the new value $L_0(H\alpha)$ of NGC 1275 removes the previous discrepancy found by Johnstone & Fabian (1988) between the star formation rates within the main region, which were inferred from the $H\alpha$ luminosity and the mass deposition X-ray profile: the former was a factor of 3 larger than the latter. The luminosity of the main region (Table 3) implies SFR $\sim 10 h^{-2} M_\odot \text{ yr}^{-1}$, in agreement with the mass deposition rate of X-ray gas in the main region, $\dot{M}_X \sim 7.5\text{--}15 h^{-2} M_\odot \text{ yr}^{-1}$ (Johnstone & Fabian 1988). Therefore, the hypothesis of a low-mass cutoff to the IMF at $2 M_\odot$, which had been used to reconcile the two estimates of the star formation rate by Johnstone & Fabian, is not needed in the comparison of the star formation rates derived from the $H\alpha$ and X-ray flux measurements of NGC 1275.

We conclude that, based on the $H\alpha$ data presented in this paper, the situation in NGC 1275 seems to be less complicated than before; a normal IMF for star formation in the central galaxy does not contradict the data. The same conclusion has been reached in another massive cooling flow, A1795 (Johnstone & Fabian 1988). Finally, these results lead to a lower value, $H_{\text{rec}} \sim 550$, for NGC 1275, where H_{rec} is the number of recombinations per H^+ ion needed for the total mass deposition rate of X-ray gas, $\dot{M}_X \sim 50 h^{-2} M_\odot \text{ yr}^{-1}$

(using $\dot{M}_X \propto r$ within the Perseus Cluster core radius $\sim 100 h^{-1}$ kpc; Johnstone & Fabian 1988), to be consistent with $\dot{M}_{\text{H}\alpha} \sim 2.7 \times 10^4 h^{-2} M_{\odot} \text{ yr}^{-1}$ inferred from the total extinction-corrected H α luminosity (see Fabian, Nulsen, & Canizares 1984).

5. STAR FORMATION IN THE HV SYSTEM

The HV system occupies a special location, in the central parts of the Perseus Cluster gravitational potential well, which makes it a particularly interesting probe to test various dynamical and star formation processes in this cluster. The HV system is a gas-rich galaxy, with bright H II regions, seen in projection on the line of sight to NGC 1275, and possibly, it is not interacting with the cD galaxy (Rubin et al. 1977; Keel 1983). Ram pressure could strip most gas from the HV galaxy moving in the intracluster medium (ICM) (Gunn & Gott 1972). The time scale for gas removal is rather uncertain, since the gas losses may be partially recovered by gas being released to the ISM from evolved stars in the HV galaxy (Gisler 1976, 1979; Takeda, Nulsen, and Fabian 1984). A rough estimate is given by the time taken by the HV galaxy to travel a distance equal to the cluster core radius,

$$t_c = \frac{r_c}{V} = \frac{100 h^{-1} \text{ (kpc)}}{3000 \text{ (km s}^{-1}\text{)}} = 3 \times 10^7 h^{-1} \text{ yr} . \quad (1)$$

Before this time elapses, other interactions are likely to affect the gas and stellar content of the HV system while it moves through an inhomogeneous ICM, as the extended filamentary system seen around NGC 1275 may suggest. If the filaments are evidence of thermal instabilities in the cooling flow (Fabian & Nulsen 1977), it is of interest to consider these gas clouds comoving with the cooling flow and colliding with the HV system. For instance, Hu et al. (1983) have argued that a collision of the HV system with the cooling flow near NGC 1275 releases enormous kinetic energy that may power the optical line emission in NGC 1275. As inelastic collisions modify the state of gas clouds, we investigate now the change in the HV system itself as a result of collisions with the cloud condensates in the cooling flow. Under favorable conditions, star formation may occur, and if the time scale for star formation is short enough that ram pressure stripping is unimportant, this collision mechanism may account for the observed H α luminosity of the HV blobs. Since the filaments stretch across at least $50 h^{-1}$ kpc and the cluster gas may be inhomogeneous on large scales (Fabian & Nulsen 1977), this type of collision can be considered independently of a collision of the HV system with the cD galactic disk or with the cooling flow near NGC 1275; the HV system may well be relatively distant from the NGC 1275 nucleus (Shields & Oke 1975; Kent & Sargent 1979).

Tenorio-Tagle's (1980, 1981) collision model of a gas cloud with a galactic disk can be applied to our case, where a cloud condensate collides with the HV galaxy at a large relative velocity $V = 3000 \text{ km s}^{-1}$. The model is tried for a plausible range of cloud parameters. The hot ICM has a typical gas density $n_c = 0.05 \text{ cm}^{-3}$ and a temperature $T_c = 10^8 \text{ K}$ (Kent & Sargent 1979). A multiphase ICM may also contain cooler and denser clouds in pressure equilibrium with the surrounding hot gas clouds (Matthews & Bregman 1978; Cowie, Fabian, & Nulsen 1980), e.g., clouds of $T_c = 10^6 \text{ K}$ and $n_c = 0.5 \text{ cm}^{-3}$, and of $T_c = 10^4 \text{ K}$ and $n_c = 50 \text{ cm}^{-3}$. Thermal instabilities in the cooling flow lead to the formation of large clumps (David, Bregman, & Seab 1988). We have idealized such clumps as spherical clouds of radius $R_c = 100 \text{ pc}$.

The collision scenario has been described in detail by Tenorio-Tagle (1980; see his Fig. 1 for a schematic representation). The colliding cloud travels a distance in the galactic disk about equal to its own dimension, creating a cavity filled with hot gas. A shocked layer of compressed gas is formed in the galactic disk after the passage of two shocks, one moving in the galaxy, the other moving along the opposite direction inside the colliding cloud. The collision event terminates when the shocks leave either the galaxy or the cloud; for a thick galactic disk adopted here, of scale height 1 kpc or greater, the crossing time is much shorter in the cloud than in the galaxy. The subsequent evolution depends on the densities of the unperturbed gas components, hence on the gas cooling rates. From our point of view of investigating the conditions and time scale of star formation in the HV galaxy, the collision produces thermal energy, and the hot cavity expands adiabatically, sweeping a shell of shocked gas into the neutral disk. The energy deposited in the disk is retained when the cooling time for the galactic shocked shell is less than the shocked cloud crossing time, and star formation may eventually occur. Jean's criterion determines t_j , the time when gravitational instability sets in in the shell. Star formation in the collapsed cloud follows some 1 Myr or so later (Braunsfurth & Feitzinger 1983; Dopita, Ford & Webster 1985).

Adopting Tenorio-Tagle's (1980) self-consistent method, calculations were done with a time step of $2 \times 10^4 \text{ yr}$ to determine the quasi-static changes of the thermodynamical state of the fully ionized expanding cavity.

Figures 5a–5c shows five curves which describe the relation of the important time scales with galactic density in this collision model, for several values of the colliding cloud density n_c . These are the crossing and cooling times of the shocked gas cloud and galactic disk, and the time or onset of star formation, t_j . The hatched areas exclude galactic density values too small for star formation to occur. It can be seen that stars can form in the HV clouds denser than $\sim 10 \text{ cm}^{-3}$, 1–6 Myr after the impact of ICM clouds with the galaxy. This is much shorter than the time given by equation (1) and will happen before gas stripping becomes effective. For the collision of the galaxy with ICM clouds of small density, conditions for star formation are achieved earlier, since t_j is shorter for small n_c . When the colliding cloud density increases, less of the galactic disk cools before the end of the collision, which results in the ejection of the shocked gas layer throughout the disk and no galactic star formation. Also, the expansion of the hot cavity may not be always adiabatic, owing to the reduced cooling time of the colliding shocked cloud (0.3–0.5 Myr in Fig. 5c). This cooling time has been plotted, at the time t_j , in Figures 5a–5c (short-dashed line), using

$$t_{\text{AC}} = \frac{3.45 \times 10^{-24} T_c(t_j)}{\Lambda n_c(t_j)} \text{ Myr} , \quad (2)$$

where T_c is the temperature in the cavity and Λ is the temperature-dependent cooling coefficient taken from McKee & Cowie (1977). In Figure 5c the shell expansion is slower and star formation takes longer; the cavity may refill, and star formation may not occur before the gas pressure in the compressed shell becomes less than the surrounding disk gas pressure. The average pressure of the Galactic ISM, $P_G \sim 8 \times 10^{-13} \text{ dynes cm}^{-2}$, has been adopted for the unperturbed gas in the disk.

In our model, the swept mass of gas in the galactic disk can

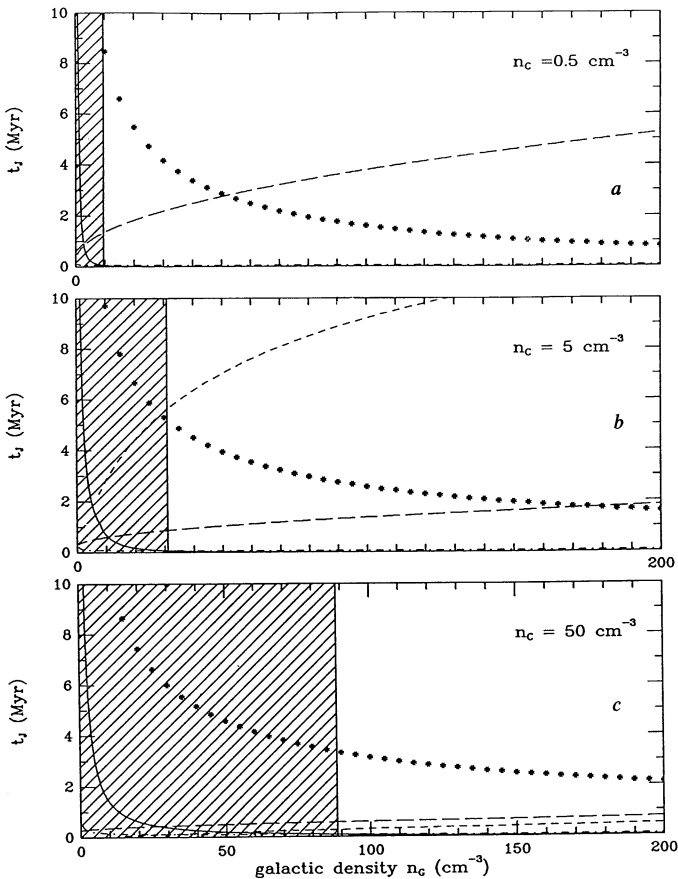


FIG. 5.—(a–c) Dependence of the time t_j on the galactic density n_G and the colliding cloud density n_c , for a cloud of radius 100 pc. The asterisk marks the time t_j at which gravitational instability sets in in the galactic shocked gas. The solid and short-dashed lines show the dependence on n_G of the cooling times of the galactic shocked gas and of the hot gas in the cavity, respectively. The long-dashed and dot-dash lines show how the dependence on n_G of the shock crossing times in 1 kpc thick galactic medium and in the cavity, respectively. Hatched areas show the ranges of n_G values that do not lead to the collapse of shocked gas and consequently to the formation of stars before the collision ends.

be approximated by

$$M_{\text{gas}} = 2.47 \times 10^{-8} \pi R(t_j)^2 \left[R(0) + \frac{w(t_j)}{2} \right] n_G \times 10^6 M_{\odot} \quad (3)$$

for a cylindrical cavity of initial radius $R(0)$ and radius $R(t_j)$ at the onset time t_j of Jeans instability, and height $w(t_j)$ (lengths in pc). The mass above the galactic disk is not included in equation (3), as the expansion of the hot cavity will occur in a less dense medium (halo) where the Jeans criterion will not be satisfied. The swept masses in Figure 6 are considerable, owing to the large volumes of the cavities blown into the disk during the collision. Realistically, the galactic disk density n_G is not constant on the length scales involved [$R(t_j) \geq 100\text{--}270 h^{-1}$ pc, $w(t_j) \sim$ several kpc]. The scenario may be that star formation occurs in dense clumps of several hundred parsecs. Clearly, the HV system images show aggregates of small-size H α knots (unresolved, $\sim 2'' = 500 h^{-1}$ pc each). The mass of the star clusters ionizing the observed H α knots, M_* , is obtained from the dereddened luminosities (Table 3 and Galactic $A_V = 0.54$ mag) and integration of a normalized IMF (Lequeux et al.

1981). For this IMF we used the predicted flux of Lyman continuum photons of a cluster $N_{\text{Lyc}} = 6.3 \times 10^{45}$ photons s^{-1} per M_{\odot} formed. Using a ratio of 2.2 ionizing photons per H α photon (case B recombination), the total flux of Lyman continuum photons of the star clusters ionizing the knots was estimated from the extinction-corrected H α luminosities; then it was divided by N_{Lyc} to give the total mass of the cluster. For example, the multiple knot region 7 is excited by a star cluster of $M_* \sim 4.4 \times 10^6 h^{-2} M_{\odot}$. The collision with a cloud of radius $R_C = 100$ pc and density $n_c = 0.5 \text{ cm}^{-3}$ sweeps $(1.0\text{--}2.5) \times 10^8 M_{\odot}$ of gas, enough to form such a cluster in 1–8 Myr with a star formation efficiency of $\sim 2\text{--}4 h^{-2}\%$. The star formation rate inferred from the extinction-corrected H α luminosity of knot 7 is $\text{SFR} = 0.34 h^{-2} M_{\odot} \text{ yr}^{-1}$. Assuming continuous star formation at this rate, then the cluster should be detectable during the time period $M_*/\text{SFR} = 13$ Myr. The entire HV system leads to the same estimate (total $\text{SFR} \sim 0.96 h^{-2} M_{\odot} \text{ yr}^{-1}$, $M_* \sim 12.4 \times 10^6 h^{-2} M_{\odot}$). This gives an estimate of the minimum lifetime of the HV galaxy as the observed system of H α clumps, $t_{\text{HV}} \sim 13$ Myr, if the collisions of ICM clumps with the HV galaxy occurred once, at the same time.

6. ON THE ORIGIN OF THE HV SYSTEM

In this section we reexamine the nature of the HV system, and its physical relation to NGC 1275. Two possible interpretations have been introduced. Either the HV system is a chance interloper gravitating in the Perseus Cluster, seen on the line of sight to NGC 1275; several authors have suggested that the HV system is a late-type Sc or Sd galaxy, with H II regions (Rubin et al. 1977; Kent & Sargent 1979; van Gorkom & Ekers 1983; Keel 1983). Or the HV system is interacting strongly with the cD galaxy via a direct collision between the HV and LV systems (Minkowski 1957; Cowie et al. 1983; Hu et al. 1983; Unger et al. 1990) or via jet action of the NGC 1275 nucleus upon the HV system (Meaburn et al. 1989).

The direct collision mechanism or the collision between the HV galaxy and the cooling flow near NGC 1275 provided impact energy from the HV galaxy to explain “the uniquely high H α luminosity” of the cD galaxy found by Cowie et al.

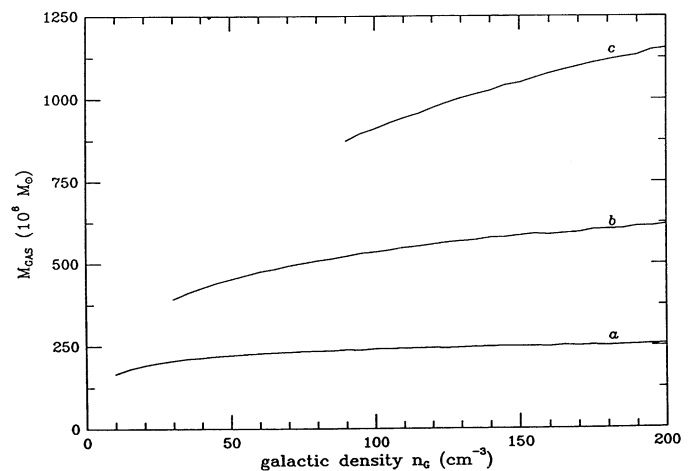


FIG. 6.—Swept mass of galactic gas, M_{gas} , as a function of n_G , given by eq. (3). For cloud density values, (a) $n_c = 0.5 \text{ cm}^{-3}$, (b) $n_c = 5 \text{ cm}^{-3}$, (c) $n_c = 50 \text{ cm}^{-3}$. The curves are not drawn for values of n_G that do not lead to the collapse of shocked gas.

(1983). However, we found NGC 1275 H α luminosity not to be as high as previously estimated by these authors.

We find that NGC 1275 is comparable to other known massive cooling flow galaxies which have no known coincident HV-type systems falling into their potential wells; therefore, the direct collision hypothesis is not required. Nevertheless, the possibility of a collision between the HV system and cooling flow aggregates and long filaments pervading the Perseus Cluster on ~ 100 kpc scale can be addressed to explain the observed H α luminosity of *the HV galaxy itself* via star formation. Our H α images of the HV system showing gaseous knots, combined with previous spectroscopic measurements (Kent & Sargent 1979; Meaburn et al. 1989), support a view in which the HV system has multiple giant H II regions excited by massive star clusters, of total SFR $\sim 1 h^{-2} M_{\odot} \text{ yr}^{-1}$, which is typical of a late or irregular Magellanic-type galaxy (Kennicutt 1983). Collisions of the HV galaxy with the cloud intracluster medium may initiate star formation 1–8 Myr after the collision, and in turn the newborn OB stars excite the surrounding gas at the observed H α luminosities of the knots. The moderate rate of star formation is able to maintain the ionization of the knots for ~ 13 Myr. To test our scenario, *IUE* observations of a very faint UV continuum can be used further to evaluate the

contribution of a hot stellar population in the HV system (Caulet, Bruhweiler, & Smith 1992). Observational constraints on its distance d relative to the background nucleus imply $d \geq 32 h^{-1}$ kpc (Shields & Oke 1975; Kent & Sargent 1979). Eventually, the HV galaxy destiny may be its cannibalization by the cD galaxy (Ostriker & Tremaine 1975).

The authors are grateful to the Operations Staff of the Steward Observatory for much assistance at the telescope, and to a generous Time Allocation Committee. We appreciate the generous allotment of telescope time and support of the Goddard 36" Telescope Facility, operated by the Laboratory for Astronomy and Solar Physics (LASP), where the Fabry-Perot imager was extensively tested before these observations. We gratefully acknowledge enlightening scientific discussions with Fred Bruhweiler, Andrew M. Smith, Richard Green, and Steve Shore. We also thank Wayne Landsman and Keith Feggans for sharing their insights on IDL that helped us develop image processing routines for Fabry-Perot data reduction and analysis. Most of this work was done while one of us (A. C.) held a National Academy of Sciences/National Research Council Research Associateship in the LASP at NASA/Goddard Space Flight Center.

REFERENCES

- Braunforth, E., & Feitzinger, J. V. 1983, *A&A*, 127, 113
 Burbidge, E. M., & Burbidge, G. R. 1965, *ApJ*, 142, 1351
 Burbidge, E. M., Smith, H. E., & Burbidge, G. R. 1978, *ApJ*, 219, 400
 Burstein, D., & Heiles, C. 1984, *ApJS*, 54, 33
 Cardelli, J. A., Clayton, G. C., & Mathis, J. S. 1989, *ApJ*, 345, 245
 Caulet, A., Bruhweiler, F. C., & Smith, A. M. 1992, in preparation
 Cowie, L. L., Fabian, A. C., & Nulsen, P. E. J. 1980, *MNRAS*, 191, 399
 Cowie, L. L., Hu, E. M., Jenkins, E. B., & York, D. G. 1983, *ApJ*, 272, 29
 David, L. P., Bregman, J. N., & Seab, C. G. 1988, *ApJ*, 329, 66
 De Young, D. S., Roberts, M. S., & Saslaw, W. C. 1973, *ApJ*, 185, 809
 Dopita, M. A., Ford, H. C., & Webster, B. L. 1985, *ApJ*, 297, 599
 Fabian, A. C., & Nulsen, P. E. J. 1977, *MNRAS*, 180, 479
 Fabian, A. C., Nulsen, P. E. J., & Canizares, C. R. 1984, 310, 733
 Gisler, G. R. 1976, *A&A*, 51, 137
 ———. 1979, *ApJ*, 228, 385
 Gunn, J. E., & Gott, J. R. 1972, *ApJ*, 176, 1
 Heckman, T. M. 1981, *ApJ*, 250, L59
 Heckman, T. M., Baum, S. A., van Breugel, W. J. M., & McCarthy, P. 1989, *ApJ*, 338, 48
 Hu, E. M., Cowie, L. L., Kaaret, P., Jenkins, E. B., York, D. G., & Roesler, F. L. 1983, *ApJ*, 275, L27
 Johnstone, R. M., & Fabian, A. C. 1988, *MNRAS*, 233, 581
 Keel, W. C. 1983, *AJ*, 88, 1579
 Kennicutt, R. C. 1983, *ApJ*, 272, 54
 Kennicutt, R. C., & Kent, S. M. 1983, *AJ*, 88, 1094
 Kent, S. M., & Sargent, W. L. W. 1979, *ApJ*, 230, 667
 Lequeux, J., Maucherat-Joubert, M., Deharveng, J. M., & Kunth, D. 1981, *A&A*, 103, 305
 Lynds, C. R. 1970, *ApJ*, 159, L151
 Massey, P., Strobel, K., Barnes, J. V., & Anderson, E. 1988, *ApJ*, 328, 315
 Mathews, W. G., & Bregman, J. N. 1978, *ApJ*, 224, 308
 McKee, C. F., & Cowie, L. L. 1977, *ApJ*, 215, 213
 Meaburn, J., Allan, P. M., Clayton, C. A., Marston, A. P., Whitehead, M. J., & Pedlar, A. 1989, *A&A*, 208, 17
 Minkowski, R. 1955, *Carnegie Yrb.*, 54, 25
 ———. 1957, in *IAU Symp. 4, Radio Astronomy*, ed. H. C. van de Hulst (Cambridge: Cambridge Univ. Press), 107
 Osterbrock, D. E. 1989, *Astrophysics of Gaseous Nebulae and Active Galactic Nuclei* (Mill Valley: University Science Books)
 Ostriker, J. P., & Tremaine, S. D. 1975, *ApJ*, 202, L113
 Romanishin, W. 1987, *ApJ*, 323, L113
 Romanishin, W., & Hintzen, P. 1988, *ApJ*, 324, L17
 Rubin, V. C., Ford, W. K., Peterson, C. J., & Oort, J. H. 1977, *ApJ*, 211, 693
 Sarazin, C. L. 1988, *X-Ray Emissions from Clusters of Galaxies* (Cambridge: Cambridge Univ. Press)
 Shields, G. A., & Oke, J. B. 1975, *PASP*, 87, 879
 Shields, J. C., & Filippenko, A. V. 1990, *ApJ*, 353, L7
 Takeda, H., Nulsen, P. E. J., & Fabian, A. C. 1984, *MNRAS*, 208, 461
 Tenorio-Tagle, G. 1980, *A&A*, 88, 61
 ———. 1981, *A&A*, 94, 338
 Unger, S. W., Taylor, K., Pedlar, A., Ghataure, H. S., Penston, M. V., & Robinson, A. 1990, *MNRAS*, 242, 33P
 van Gorkom, J. H., & Ekers, R. D. 1983, *ApJ*, 267, 528